Zeitschrift: Helvetica Physica Acta
Band: 57 (1984)
Heft: 3

Artikel: Structural dynamics in the chain compound (CH_3)_3NHCdCl_3
Autor: Walther, U. / Brinkmann, D. / Arend, H.
DOI: https://doi.org/10.5169/seals-115512

Helvetica Physica Acta, Vol. 57 (1984) 400–415

0018–0238 84 030400–16$1.50 + 0.20 0

Structural dynamics in the chain compound $(CH_3)_3NHCdCl_3$

By U. Walther[1]) and D. Brinkmann, Physik-Institut, Universität Zürich, 8001 Zürich, Switzerland
H. Arend, Laboratorium für Festkörperphysik, Eidg. Technische Hochschule, 8093 Zürich, Switzerland

(6. III. 1984)

Abstract. $(CH_3)_3NHCdCl_3$ and $(CH_3)_3NDCdCl_3$ were studied between 120 K and 440 K by proton and deuteron NMR, dielectric, and electric conductivity measurements. Activation energies and correlation times for four types of molecular motions were determined: rotations of the CH_3-group and of the organic ion, jumping of the molecule between two inequivalent sites, and diffusion along the chains. A possible arrangement of the chains around the 342 K phase transition is discussed.

I. Introduction

Solids with pronounced one-dimensional (1D) properties have attracted considerable interest for a long time. While many investigations were devoted to the 1D aspect of magnetism and electronic conductivity, less attention has been paid to compounds where 1D properties show up only in structural aspects. To this class of materials belongs trimethyl-ammonium cadmium chloride, $(CH_3)_3NHCdCl_3$ (short TrMCd) which consists (Fig. 1) of infinite chains of face-sharing $CdCl_6$ octahedra and $(CH_3)_3N$ ions occupying the space between the chains and forming N—H · · · Cl hydrogen bonds [1].

In the first investigation of TrMCd [1] employing X-ray diffraction, nuclear magnetic resonance (NMR), and differential thermal analysis (DTA), three successive structural phase transitions at 342 K, 374 K, and 415 K were detected and it was realized that the dynamics of the organic group plays a major role in these phase transitions. The reorientational dynamics of the $(CH_3)_3NH$ groups and the rotary modes of the $CdCl_6$ octahedra were investigated by Raman spectroscopy [2]. Subsequent calorimetry, thermal expansion, and X-ray diffraction studies [3, 4] revealed the structure of the room temperature phase (orthorhombic, space group Pbnm) and showed that the two high-temperature phases existing below 415 K are hexagonal (space group $P6_3/m$). The symmetries of the order parameters of these phase transitions were investigated by means of group theory [5]. Instead of the hexagonal space group, recent X-ray diffraction, polarizing-microscope, and dilatometric studies [6, 7] have assigned the orthorhombic space

[1]) Present address: Oberallenbergstrasse, 8708 Männedorf, Switzerland.

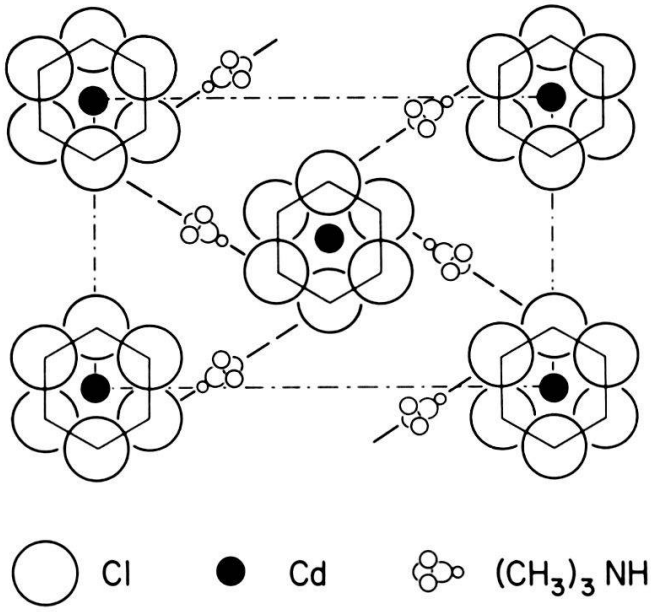

Figure 1
Structure of $(CH_3)_3HNCdCl_3$ at room temperature, projection along the c axis showing only part of $CdCl_6$ octahedra. Hydrogen bonds are indicated by dashed lines.

group Pbnm to the high-temperature phase which exists between 342 K and 374 K.

In contrast to the studies just mentioned [2–7], the present paper which is mainly based on the thesis [8] of one of us (U.W.) reports on NMR, dielectric, and electric conductivity experiments which were performed to get information on activation energies and correlation times of the various molecular motions in TrMCd. The computer controlled dielectric measurements are described in some detail. The results of the deuteron NMR allow to propose a model for the arrangement of the Cl columns in the 342 K to 374 K phase, this model is consistent with a hexagonal structure of this phase.

The TrMCd samples used for these investigations were prepared as follows. Since TrMCd is congruently soluble in water, seed crystals were obtained from slightly acidified (HCl) aqueous solutions by slow cooling or evaporation. Starting from these seeds, crystals with a volume of several cm^3 were grown by slow cooling of stirred saturated solutions from approximately 320 K down to room temperature.

II. NMR

Two types of NMR experiments were performed: a study of (i) the proton resonance in regular and deuterated TrMCd and (ii) of the deuteron resonance in deuterated TrMCd. All experiments were carried out with a Bruker SXP pulse spectrometer. The signals were digitized by a transient recorder and accumulated and Fourier transformed by an on-line computer. Signal positions were determined from the Fourier transform of the free-induction decay (FID) signal following a $\pi/2$ radio-frequency pulse. To measure the spin-lattice relaxation time T_1 of signals which are broad or exhibit a fine structure, the saturation method

was employed: A sequence of several $\pi/2$ pulses is applied to the sample in order to totally saturate the NMR line. The subsequent recovery of the signal is measured by means of a $\pi/2$ pulse. The T_1 of narrow signals was determined by a $\pi - \pi/2$ pulse sequence.

Probe temperatures were monitored within ± 0.5 K by means of thermocouples and platinum resistors. However, the main error arises from temperature gradients over the sample which can reach a few degrees in the case of powder samples due to the additional heating caused by the radio-frequency pulses.

II(A). Proton NMR

The proton absorption signal obtained from single crystals at room temperature has an almost perfect Gaussian lineshape. However, as shown in Fig. 2, at lower temperatures the signal exhibits a fine structure and at 80 K a triplet structure is clearly identified with separations between the components depending on the orientation of the sample.

The triplet structure can be interpreted by assuming rapid rotations of the CH_3-groups around their symmetry axis. For an individual CH_3-group this rotation averages the magnetic dipole–dipole interaction between the three hydrogen nuclei which have spin $\frac{1}{2}$. As a result a triplet is observed with the central signal appearing at the Larmor frequency ν_L flanked by two satellite signals at frequencies [9]

$$\nu_L \pm \frac{3}{2}\frac{\mu_0 \gamma}{2\pi r^3}(3\cos^2\theta - 1)$$

Here, r is the interproton distance within a CH_3-group, θ is the angle between the external field and the rotation axis, μ_0 is the nuclear Bohr magneton and γ is the magnetogyric ratio of the proton. In a single crystal there is a distribution of the

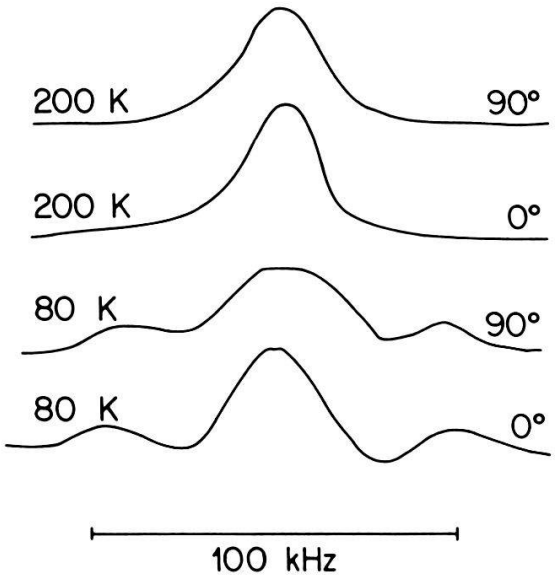

Figure 2
Proton NMR signal in a $(CH_3)_3HNCdCl_3$ single crystal at 80 K and 200 K with the c-axis perpendicular to the magnetic field and two arbitrary orientations of the a-axis differing by 90°.

angle θ and hence an overlap of several triplets resulting in the observed spectrum.

Details of the dynamics of the CH_3-group may be revealed by measuring the spin-lattice relaxation time T_1. This is the time constant of the approach of the nuclear spins to thermal equilibrium with the "lattice" which comprises all other degrees of freedom of a material such as molecular rotations, phonons, diffusion etc. If the local magnetic (and electric) fields at the nuclear sites arising from the lattice dynamics fluctuate strongly at the Larmor frequency, relaxation is strong and T_1 is short.

The proton T_1 has been measured in both single crystals and powder samples. For temperatures between 77 K and 365 K the anisotropy of T_1 is 10% at most. At 300 K and 90 MHz the average T_1 is $0.28 \pm 0.03s$ which agrees fairly well with the value obtained in a powder. Furthermore, no significant difference between deuterated and non-deuterated samples could be detected. For a further discussion we consider only the relaxation rate in a deuterated powder sample. The temperature dependence of $1/T_1$ for two values of the Larmor frequency is given in Fig. 3.

The data are interpreted in terms of a composite motion of the $(CH_3)_3$ ND-unit consisting of a rotation of the CH_3-group about its three-fold axis, a hindered rotation of the $(CH_3)_3$ ND-unit about its three-fold axis along the ND-bond, and an isotropic tumbling of the whole unit. Each type of motion causes a fluctuating magnetic field at the site of a proton. We assume an exponential decay of the corresponding correlation functions with correlation times τ_c for the CH_3 rotation, τ_{c2} for the hindered rotation, and τ_{c1} for tumbling. Then the relaxation rate can be written as [10]

$$\frac{1}{T_1} = \frac{9}{80} \frac{\gamma^4 \hbar^2}{r^6} [Af(\tau_{c1}) + Bf(\tau_{c3}) + Cf(\tau_{c4}) + Df(\tau_{c5})]$$

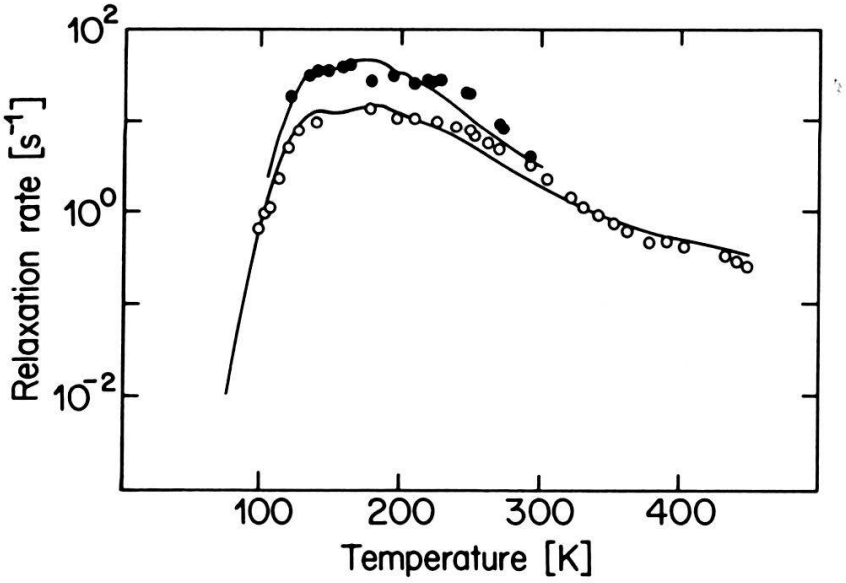

Figure 3
Temperature dependence of the proton relaxation rate in $(CH_3)_3NDCdCl_3$ powder at 32 MHz (full circles) and 90 MHz (open circles). The lines represent a fit of equation (1) to the data.

where

$$f(\tau) = \frac{\tau}{1+\omega^2\tau^2} + \frac{4\tau}{1+4\omega^2\tau^2}$$

and

$$A = \tfrac{1}{3}(1-3\cos^2\delta)^2, \qquad B = \tfrac{3}{2}\sin^2\delta$$
$$C = \sin^2 2\delta + \sin^4\delta, \qquad D = \tfrac{1}{2}(8-3\sin^4\delta)$$

where δ is the angle between the C—N-bond and the three-fold axis of the whole unit, and

$$\frac{1}{\tau_{c3}} = \frac{1}{\tau_{c1}} + \frac{1}{\tau_c}, \qquad \frac{1}{\tau_{c4}} = \frac{1}{\tau_{c1}} + \frac{1}{\tau_{c2}}, \qquad \frac{1}{\tau_{c5}} = \frac{1}{\tau_{c1}} + \frac{1}{\tau_c} + \frac{1}{\tau_{c2}}$$

Again, r is the interproton distance within a methyl group. With $r = 1.8$ Å and $\delta = 75°$ [11] one obtains

$$\frac{1}{T_1} = 1.67 \cdot 10^{10}[0.024 f(\tau_{c1}) + 1.306 f(\tau_{c3}) + 1.121 f(\tau_{c4}) + 2.694 f(\tau_{c5})] \tag{1}$$

It is natural to assume that each of the correlation times τ_c, τ_{c1}, and τ_{c2} follows an Arrhenius law $1/\tau = (1/\tau_0)\exp(-E/kT)$ where E is an activation energy and $1/\tau_0$ the "prefactor". However, it turned out that the experimental data could not be fitted by equation (1) if, at each temperature, single values for τ_c, τ_{c1}, and τ_{c2} are assumed. The "width" of the fitted curve near the $1/T_1$ maximum is smaller than the width of the experimental curve. However, assuming a distribution of τ values for each temperature a reasonable fit can be accomplished. Such a distribution is suggested because below room temperature the recovery of the nuclear magnetization is non-exponential, i.e. not-describable by a single T_1 value. Physically this means that different $(CH_3)_3$ ND-units in the crystal perform slightly different rotations. For simplicity a logarithmic Gaussian distribution was assumed given by

$$p(\tau) = \frac{1}{\sigma\sqrt{\pi}} \exp\left[-\frac{(\ln\tau - \ln\tau_0)^2}{2\sigma^2}\right] \tag{2}$$

Since the experimental errors did not allow to distinguish different values of σ, the same value of σ was chosen for all four distribution functions. Details of the evaluation are described in Ref. [8]. The results of the fit are summarized in Table 1, they will be discussed in Section 5.

Table 1
Prefactors and activation energies of the correlation times of the four types of molecular motions in $(CH_3)_3NHCdCl_3$.

	Prefactor [s]	Activation energy [eV]
CH_3-rotation	$2\times10^{-13}\pm20\%$	$0.125\pm10\%$
Rotations around N—C-bond	$5\times10^{-14}\pm50\%$	$0.19\ \pm20\%$
Two-sites jumping	$1\times10^{-17}\pm15\%$	$0.70\ \pm\ 3\%$
Diffusion along c-axis	$8\times10^{-20}\pm50\%$	$1.2\ \ \pm15\%$

II(B). Deuteron NMR

The electric quadrupole moment eQ of the deuteron interacts with inhomogeneous electric crystal fields causing a splitting of the resonance line. Thus deuteron NMR is apt to probe the electric field gradient (EFG) tensor at a nuclear site. If the components of this tensor along its principal axes are denoted by V_{ii}, it is customary to label the axes so that

$$|V_{zz}| \geq |V_{yy}| \geq |V_{xx}|$$

If the tensor is axially symmetric, i.e. $V_{xx} = V_{yy}$, the EFG tensor is completely specified, besides its orientation, by V_{zz}. NMR yields the so-called quadrupole coupling constant eQV_{zz}/h which has the dimension of a frequency.

If the coupling constant is small as compared to the Larmor frequency ν_L the quadrupole interaction can be treated as a perturbation of the Zeeman interaction yielding a splitting of the deuteron resonance signal into a doublet with frequencies [12]

$$\nu = \nu_L \pm \tfrac{1}{4}\nu_Q(3\cos^2\theta - 1) + \frac{1}{8}\frac{\nu_Q^2}{\nu_L}(\sin^2\theta\cos^2\theta + \tfrac{1}{4}\sin^4\theta) \tag{3}$$

where θ is the angle between the V_{zz} direction and the magnetic field and $\nu_Q = \frac{3}{2}(eQV_{zz}/h)$. By measuring the doublet separation as a function of θ the coupling constant is obtained.

In Fig. 4(a) we have plotted the deuteron rotation pattern measured in $(CH_3)_3NDCdCl_3$ at 320 K, if the c axis is perpendicular to the magnetic field. In addition, the spectrum for 158° is shown (the zero is arbitrary). Between 280 K and the phase transition at 342 K, the rotation pattern is nearly temperature independent. Apart from the fine structure of the signals the rotation pattern consists of two identical doublets shifted against each other by 70°. The pattern can be fitted by equation (3) which yields the solid line in Fig. 4. If we interpret the fine structure as evidence for two slightly different EFG tensors we arrive at the result that in terms of the EFG the unit cell contains four different deuterium sites. For all of them, the directions of the V_{zz} components lie in the ab plane. Two of them make an angle of about 180° in the ab plane and their quadrupole coupling constants are 158.8 kHz and 162.8 kHz, the two others have the same coupling constants but their V_{zz} directions are shifted by 70° with respect to the other pair. In some crystals a third pair of EFG tensors was found with the same coupling constants but their V_{zz} directions shifted by about 64° against the second pair. So there are three pairs of EFG tensors whose V_{zz} directions are centered at 0°, 70°, and 133° where the zero is arbitrary.

At the 342 K phase transition each of the three pairs of signals of the low-temperature phase is split into a doublet each signal again with a fine structure. The corresponding rotation pattern is given in Fig. 4(b) and the orientations of the V_{zz} directions are plotted in Fig. 5. The coupling constants which correspond to the fine structure are now 157.6 kHz and 161.6 kHz, they differ only slightly from those of the low-temperature phase.

We attribute the fine structure of the deuteron signal to a back and forth jumping of the organic ion between two potential wells of depth E_1 and E_2, respectively, where the deuteron experiences slightly different field gradients. This

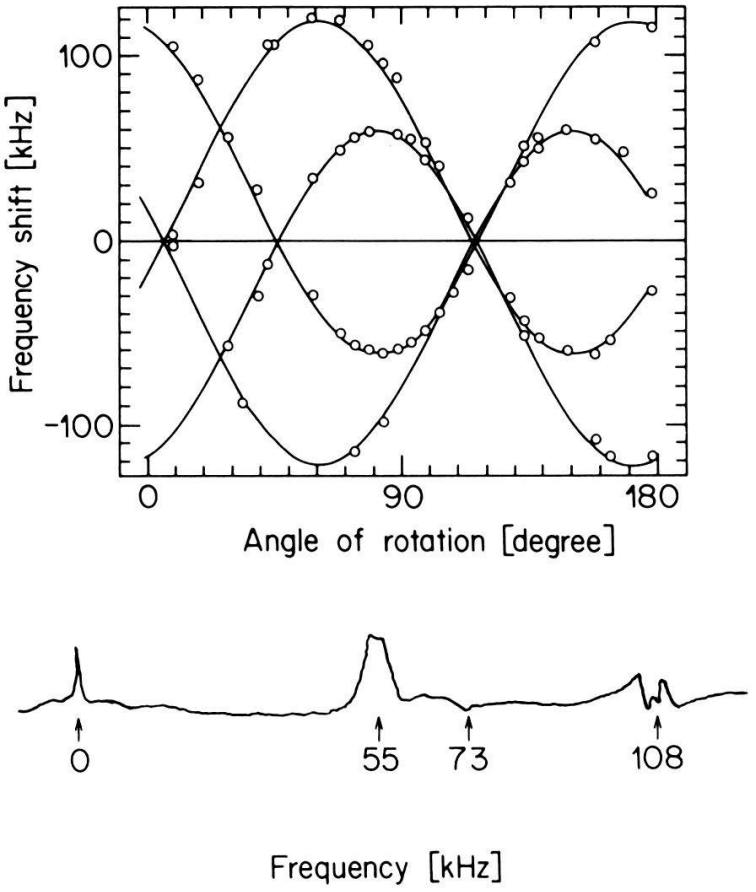

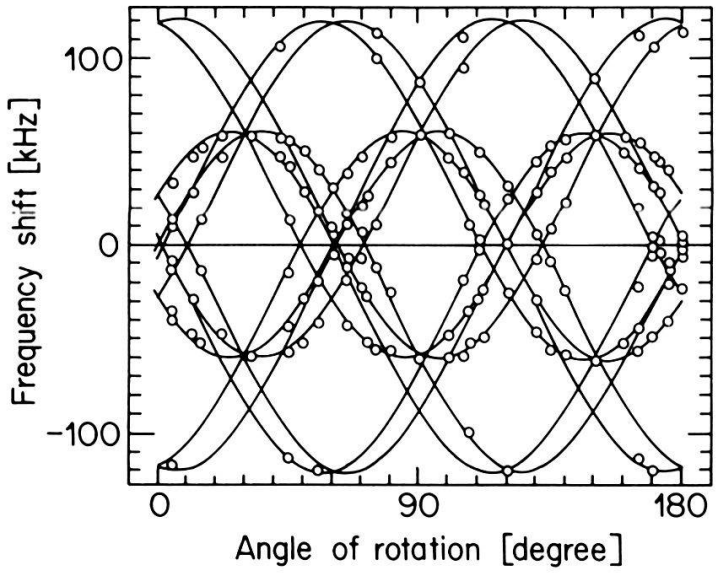

Figure 4
Shift of the deuteron NMR signals in $(CH_3)_3NDCdCl_3$ with respect to the Larmor frequency for a rotation around the c-axis. The zero of the angle of rotation is arbitrary. Solid lines are fits of equation (3) to the data. (a) Pattern at 320 K together with the spectrum at 158°. (b) Pattern at 366 K.

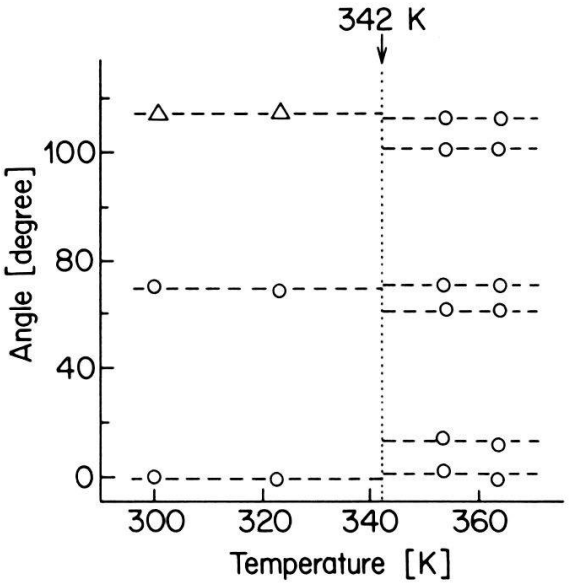

Figure 5
Orientation of the V_{zz} component of the electric field gradient at the deuteron site with respect to an arbitrary direction in the *ab* plane in $(CH_3)_3NDCdCl_3$. ○: observed in all specimens, △: observed in only some of the samples investigated.

interpretation will be more firmly supported by measurements of the dielectric relaxation (Section III). Such a fluctuating quadrupole interaction can be a powerful relaxation mechanism and can dominate the dipole–dipole relaxation discussed above. The jump process is described by a correlation time defined by

$$\frac{1}{\tau_c} = W_{12} + W_{21} = (1+a)\,W_{12}$$

W_{12} and W_{21} are the probabilities per unit time for a deuteron to jump from site 1 to 2 and vice versa. Further, $a = W_{21}/W_{12} = \exp[(E_2 - E_1)/kT]$. Explicit expressions for the relaxation rate arising from such a jump mechanism have been derived for deuterons in ferroelectrics of the KDP type [13]. If $2\pi\nu_L\tau_c \ll 1$, the relaxation rate becomes

$$\frac{1}{T_1} = \pi^2\left(\frac{eQ}{h}\right)^2 [(\Delta V_{x'y'})^2 + (\Delta V_{y'z'})^2(\sin^2\theta + 4\cos^2\theta)]\frac{a}{(1+a)^2}\tau_c \qquad (4)$$

where the $\Delta V_{x'y'}$ and $\Delta V_{y'z'}$ are the differences of components of the EFG tensors at sites 1 and 2, expressed in a crystal fixed frame, and θ is the angle between x' and the magnetic field. Since these components could not be determined experimentally equation (4) can only be used for an order of magnitude calculation of τ_c. Furthermore, each measurement of T_1 involves several values of θ. However, $eQV_{x'y'}/h$ and $eQV_{y'z'}/h$ are of the order of the coupling constant eQV_{zz}/h. Assuming this and using $a \approx 1$, $\sin^2\theta + 4\cos^2\theta \approx 3$, and the experimental value $T_1 = 0.28s$ we obtain from equation (4) $\tau_c \approx 2 \cdot 10^{-8}s$ as a lower limit for the correlation time.

III. Dielectric experiments

These experiments dealt with the real part ε' of the complex dielectric constant $\varepsilon = \varepsilon' - i\varepsilon''$. ε' has been determined as a function of both temperature T and frequency ω in two different arrangements.

In order to measure $\varepsilon(T)$ at a fixed frequency, the sample formed a capacitor parallel to a constant capacitor of about 50 to 500 pF. The sample is charged to a voltage of about 1 V amplitude with a frequency in the range 100 Hz to 100 kHz. The rectified output voltage was amplified and plotted as a function of temperature. Data were taken at both increasing and decreasing temperatures in order to eliminate errors introduced by the different heat capacities of the sample and the sensor. The results are given in Fig. 6 for four different frequencies.

The frequency dependence of the dielectric constant $\varepsilon'(\nu)$ at fixed temperature was measured by means of a computer controlled device described in detail in the Appendix. The sample forms part of an oscillator circuit whose resonance frequency is measured. The results are shown in Fig. 7. This device covers a frequency range from 50 kHz to 200 MHz thus favorably supplementing the integrator system.

In the presence of relaxation effects which may arise from the jumping of the ions between two inequivalent potential wells as introduced in Section II(B), the real and imaginary parts of the complex dielectric constant are given by the Debye equation:

$$\varepsilon' = \varepsilon_\infty + \frac{\varepsilon_0 - \varepsilon_\infty}{1 + \omega^2\tau^2}, \qquad \varepsilon'' = \frac{(\varepsilon_0 - \varepsilon_\infty)\omega\tau}{1 + \omega^2\tau^2} \tag{5}$$

where $\varepsilon_0 = \varepsilon(\omega = 0)$, $\varepsilon_\infty = \varepsilon(\omega = \infty)$, and τ is the relaxation time. However, it is not possible to fit the data of Fig. 7 by equation (5) employing a single or two

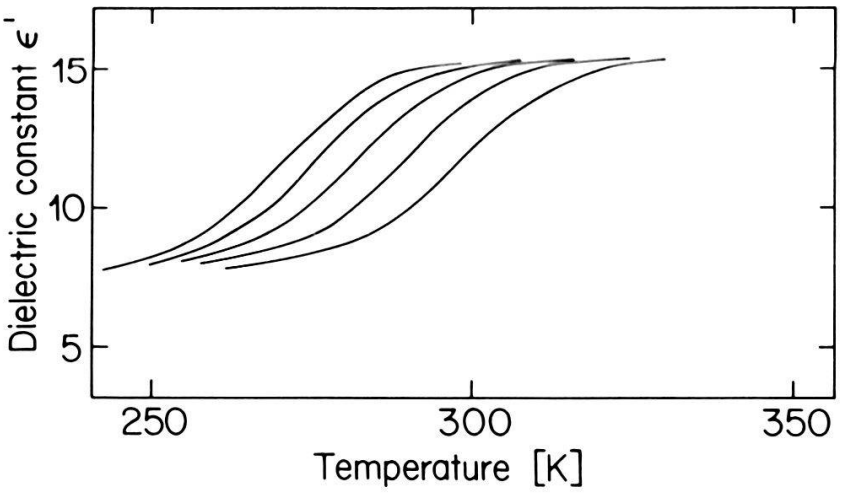

Figure 6
Temperature dependence of the dielectric constant in $(CH_3)_3NDCdCl_3$ at 0.7, 1.5, 3, 6, and 12 kHz (from left to right). The electric field is parallel to the a-axis.

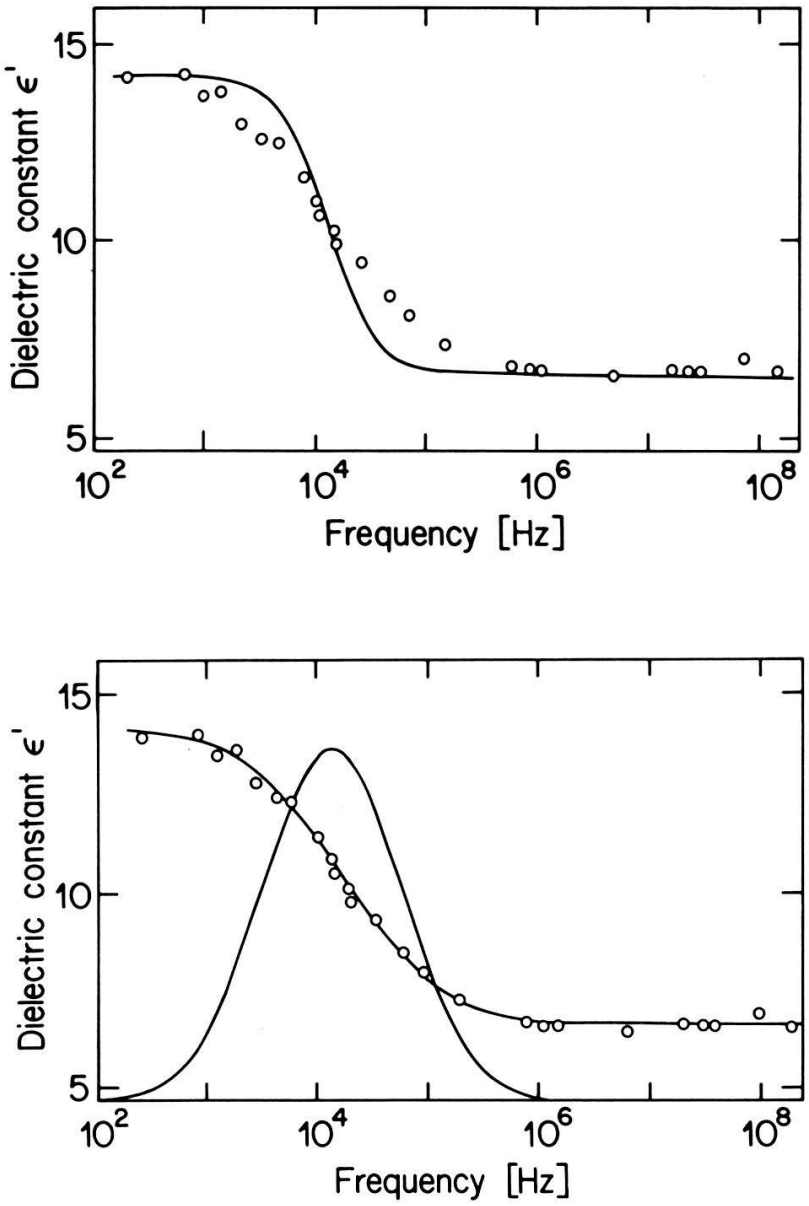

Figure 7
Frequency dependence of the dielectric constant in $(CH_3)_3NDCdCl_3$ at 297 K with the electric field parallel to the a-axis. (a) The solid line shows the unsatisfactory fit of equation (5) to the data. (b) Fit of equation (7) to the data. The Gaussian is a plot of equation (6).

relaxation times. Instead, assuming a logarithmic Gaussian distribution of relaxation times according to

$$p(\ln \tau) = \frac{1}{\sigma\sqrt{2\pi}} \exp\left[-\frac{(\ln \tau - \ln \tau_0)^2}{2\sigma^2}\right] \tag{6}$$

and replacing ε' of equation (5) by

$$\varepsilon' = \varepsilon_\infty + (\varepsilon_0 - \varepsilon_\infty) \int_0^\infty \frac{p(\ln \tau)}{1+\omega^2\tau^2}\, d\tau \tag{7}$$

provides a satisfactory fit as shown by the solid line in Fig. 7(b). In the same figure we have also plotted the distribution function $p(\ln \tau)$ since each value of τ corresponds to a frequency $1/(2\pi\tau)$. The fit of equation (7) to the experimental data is obtained for the maximum of $p(\tau)$ occurring at $\tau_0 = 11.5\ \mu s$ and the points of maximum slope at 2.8 μs and 48 μs, respectively, which determines the standard deviation σ.

The relaxation times τ thus obtained are so-called mean-field relaxation times which are related to the microscopic relaxation times τ_{mic} by the relation [14]

$$\tau_{mic} = \tau \frac{\varepsilon_\infty + 2}{\varepsilon_0 + 2} \tag{8}$$

These results are plotted in Fig. 8, together with the value $\tau_c = 2 \times 10^{-8}$ s obtained from deuteron NMR relaxation at 365 K. Since this value τ_c agrees with the extrapolation of the dielectric relaxation times to higher temperatures, we conclude that both dielectric relaxation and quadrupole relaxation arise from the same mechanism, i.e. the back and forth jumping of the organic ion between two inequivalent sites.

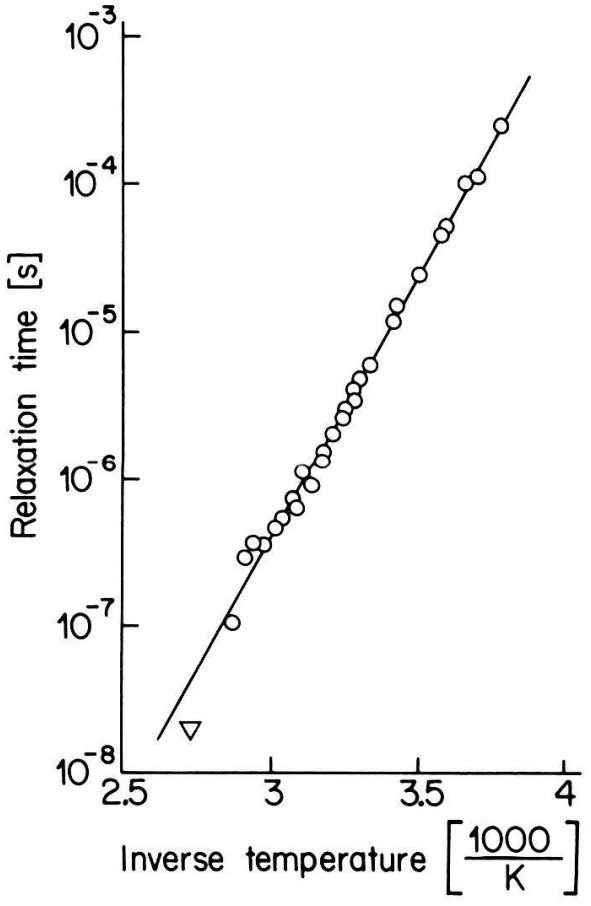

Figure 8
Temperature dependence of the mean-field dielectric relaxation time as defined by equation (8) in $(CH_3)_3NDCdCl_3$. ▽ denotes the value obtained from deuteron NMR relaxation.

IV. Measurements of electric conductivity and index of refraction

The NMR and dielectric experiments were supplemented by measuring the electric conductivity σ and the index of refraction n. Since the samples are very sensitive to heat gradients which cause cracks, only small samples were investigated and for geometrical reasons, the two-electrode method for measuring σ was employed: a variable voltage is applied to the sample, from its geometry and by measuring the current the conductivity is obtained.

The conductivity of TrMCd turned out to be highly anisotropic. The conductivity $\sigma_\perp$ perpendicular to the c axis lies in the range 10^{-14} to $10^{-16}\,(\Omega m)^{-1}$ for temperatures between 300 K and 330 K. The conductivity $\sigma_\parallel$ along the c axis is about two orders of magnitude higher than $\sigma_\perp$ with a relatively sharp increase at temperatures between 300 K and 335 K. Figure 9 shows the temperature dependence of $\sigma_\parallel T$ for two different samples. The product obeys an Arrhenius law with an average activation energy of about 1.2 eV.

The data are interpreted in terms of a quasi-one-dimensional conduction of the organic ions along the c axis. It is unlikely that conduction arises from Cl ions since no free sites are available for them; furthermore, X-ray investigations [3, 4] did not detect Cl ions on interstitial sites. Finally, Cd diffusion is highly implausible since these ions are tightly bound in the structural network. The experimental results would be compatible with an electronic conduction, but this is very

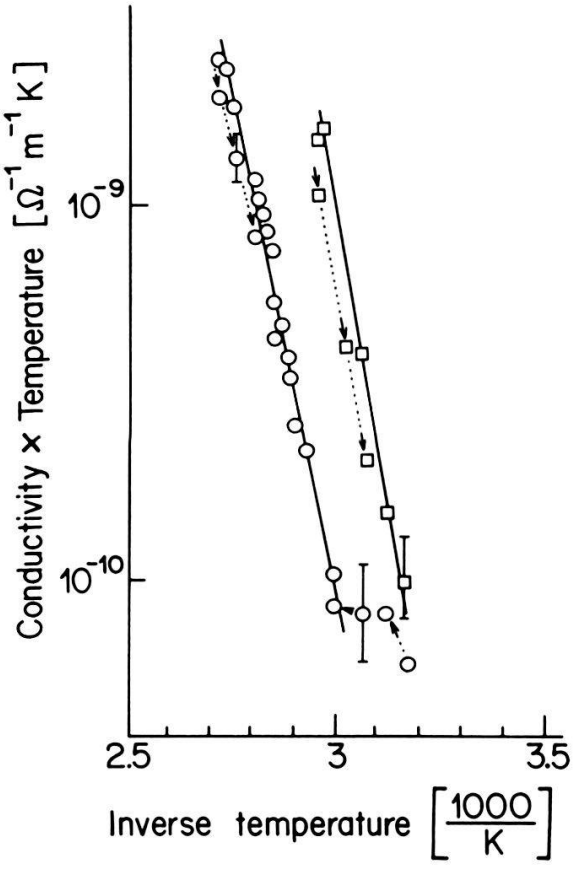

Figure 9
Conductivity × temperature as a function of inverse temperature in $(CH_3)_3NHCdCl_3$ for the electric field parallel to the c-axis. The arrows denote the sequence of the measurements. ○ and □ refer to two different samples.

unlikely in a very transparent crystal. Thus we conclude that conduction arises from the mobility of the organic ions.

Because of its orthorhombic symmetry, three indices of refraction are expected corresponding to the orthorhombic axes. At 300 K and at a wavelength of 633 nm (He–Ne laser) two distinct indices for propagation along c and perpendicular to c could be measured. These values are $n_1 = 1.682$ and $n_2 = 1.632$. Since the crystals were not oriented by X-rays, no assignment of the indices to the two orientations in question is possible. However, the difference $|n_2 - n_1| = 0.054$ shows that the birefringence is quite high in TrMCd.

V. Discussion and conclusions

From the proton relaxation data (Section II(A)) three types of motion were inferred: rotations of the CH_3-group, rotations of the organic ion around the N—C-bond, and a tumbling motion of the whole unit. On the basis of the deuteron line splitting, the deuteron relaxation (Section II(B)) was interpreted in terms of a back and forth jumping of the organic ion between two potential wells. Such a motion had been suggested by Chapuis and Zuñiga on the basis of X-ray studies [3]. While the deuteron relaxation data by themselves are not conclusive, they yield a correlation time which fits into the temperature dependence of the dielectric relaxation times. Since the dielectric relaxation as discussed above, results most likely from movements of the organic ion, both experiments are in accord with each other.

According to Ref. [3] the occupation probabilities of the two potential wells at room temperature are 0.25 and 0.75. If we assume a Boltzmann distribution of the occupation, the potential wells must differ by 0.028 eV. Together with the activation energy of 0.70 eV which we have obtained from the dielectric relaxation, one calculates a 4% asymmetry of the potential wells.

Table 1 summarizes the four different types of motion we have detected by NMR, dielectric, and conductivity experiments. The activation energies found differ by an order of magnitude and reflect the different hindrance with which these motions are performed. The prefactors τ_0 are unusually low and cannot be interpreted as the inverse of a so-called attempt frequency. $1/\tau_0$ may be written as a product $\nu_0 C$ where ν_0 is an attempt frequency and C is a factor related to the actual shape of the potential well. However, the experiment only yields the product $\nu_0 C$.

The jumping of the organic ion between two sites seems to play a central role in triggering the phase transition at $T_c = 342$ K. The increase of the jump frequency upon approaching T_c from below tends to equalize the occupation probabilities of the two sites and hence to increase the total electrostatic repulsion between ions located in opposite potential wells. Obviously this is the reason for the strong expansion of the crystal in the b direction [8]. Finally, at T_c the crystal transforms into the hexagonal structure which is energetically more favorable.

On the basis of the present deuteron FGT data we suggest the following model [8] for the arrangement of the Cl columns at temperatures around $T_c = 342$ K. Below T_c, three FGT symmetry axes each with a fine structure were determined which all lie in the ab plane. Two of these axes coincide with the direction of the D—Cl bond [3] and correspond to an orientation of the organic

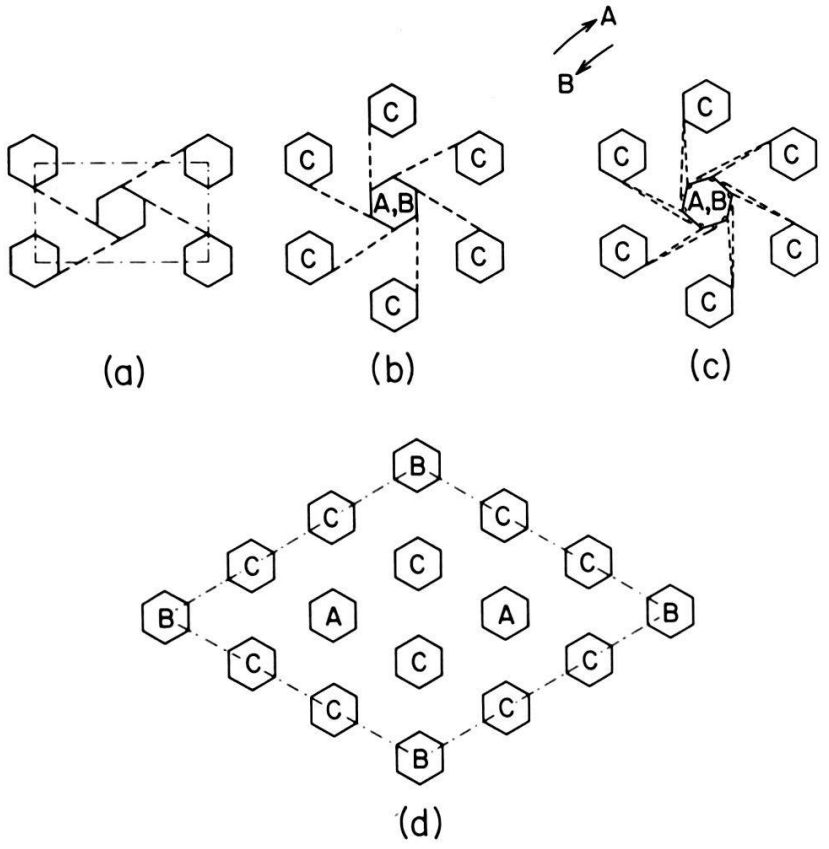

Figure 10
Schematic representation of the $CdCl_6$ columns in $(CH_3)_3NDCdCl_3$. Positions of the organic ions are indicated by dashed lines. (a) About 300 K. (b) $300 < T < 342$ K. (c) At 342 K: twist of the A and B columns with respect to each other. (d) Possible arrangement of the 3 types of $CdCl_6$ columns above 342 K.

ion as indicated by dashed lines in Fig. 10(a). The fine structure of each direction corresponds to slightly different quadrupole coupling constants of each bond. Thus in the orthorhombic phase each Cl column is bonded to four nearest Cl-columns. The third FGT-direction which could be detected in some specimens already below T_c must then correspond to an additional D—Cl bond as indicated in Fig. 10(b). Thus we have a mixture of two orthorhombic configurations, i.e. two types of columns, called A and B, respectively. At T_c, columns A and B are twisted against each other as indicated in Fig. 10(c) and three different orientations of Cl columns must be distinguished which are now called A, B, and C. Each of the A and B columns is surrounded by six C columns. This model is consistent with a hexagonal space group [3, 4] provided our specimens are one-domain single crystals; agreement with an orthorhombic space group seems to be feasible only in the presence of a multi-domain structure.

Acknowledgment

We thank Dr. G. Chapuis for valuable discussions and the Schweizerischer Nationalfonds for financial support.

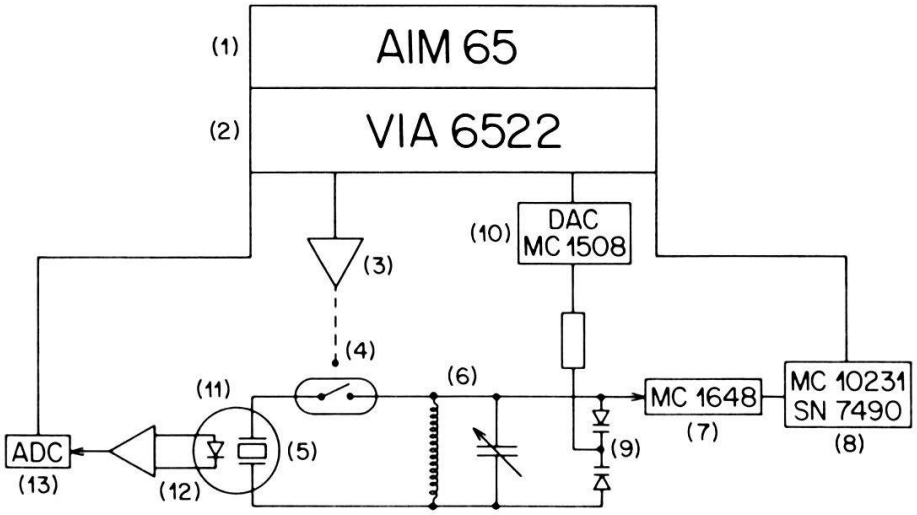

Figure 11
Block diagram of the computer controlled device for measuring the dielectric constant. Components are described in the Appendix.

Appendix: The computer controlled dielectric measurement (Fig. 11)

(a) *Hardware*

The AIM65 Computer (1) drives with its interface adapter (2) (VIA6522) a single stage transistor amplifier (3) operating a low capacity (0.5 pF) reed relay (4) connecting the sample (5) to the tank circuit (6) of an oscillator (MC1648) (7). A six stage divider (MC10231, SN7490) (8) reduces the frequency of the square wave at the output of the MC1648 by a factor of 1600 and drives the counter on the VIA6522. The frequency range is determined by the value of the inductor used. Two varactor diodes (9) provide a variable frequency input under control of a digital-to-analog converter (MC1508) (10). The sample is located in a polyethylene tube (11). A specific temperature is maintained by the gas flow of a Varian temperature controller and monitored by amplifying the voltage drop of a current driven LED (12). This voltage is fed to a successive approximation analog-to-digital converter (MC1508, LM311) (13) controlled by the computer.

(b) *Software*

To run an experiment, two programs both written in BASIC and both interrupted by assembler subroutines operate in succession. The first one calculates and stores the frequency, temperature and capacity values. Each of these values can be displayed on the LED of the AIM computer or can be continuously printed out on the printer. This program is interrupted at exact 1 ms intervals (1000 clock pulses) by an assembler language subroutine reading the counter and controlling the reed relay and the AD and DA converters.

After completion of the measurement process the second BASIC program is read in from tape (an ordinary UHER tape recorder). This program calculates the Debye function with a logarithmic Gaussian distribution of relaxation times by

overlapping several functions (usually nine) as given by equation (5) multiplied by amplitudes according to equation (6). The resulting function $\varepsilon'(\omega)$ can be displayed on an oscilloscope or plotted on an analog x–y recorder together with the measured values. This is done with an assembler subroutine interrupting the main program and feeding the two DA converters with one pair of x and y values at a time. The parameters of $\varepsilon'(\omega)$ can be changed by typing in new values until a satisfactory fit is reached. Final values for ε_0, ε_∞ and the relaxation times were obtained with another program doing a least squares fit.

REFERENCES

[1] U. WALTHER, D. BRINKMANN, G. CHAPUIS and H. AREND, Solid State Commun. *27*, 901 (1978).
[2] Y. MLIK, A. DAOUD and M. COUZI, Phys. Status Solidi (a) *52*, 175 (1979).
[3] G. CHAPUIS and F. J. ZUÑIGA, Acta Crystallogr. *B36*, 807 (1980).
[4] F. J. ZUÑIGA, Doctoral thesis, Universidad del Pais Vasco, Bilbao, Spain (1980).
[5] F. J. ZUÑIGA, G. CHAPUIS, J. L. MAÑES, J. M. PEREZ-MATO and M. J. TELLO, J. Physics *C15*, 5195 (1982).
[6] S. KASHIDA, K. SANO, T. FUKUMOTO, H. KAGA and M. MORI, J. Phys. Soc. Japan *52*, 1255 (1983).
[7] T. FUKUMOTO, K. SANO, S. KASHIDA and H. KAGA, J. Phys. Soc. Japan *52*, 4213 (1983).
[8] U. WALTHER, Doctoral thesis, University of Zürich, Switzerland (1982), available on request.
[9] E. R. ANDREW and R. BERSOHN, J. Chem. Physics *18*, 159 (1950).
[10] M. B. DUNN and C. A. MCDOWELL, Molecular Physics *24*, 969 (1972).
[11] M. F. FROIX, Phys. Rev. *B18*, 2046 (1978).
[12] A. ABRAGAM, *The Principles of Nuclear Magnetism*, Clarendon, Oxford (1961).
[13] R. BLINC, in: *Advances in Magnetic Resonance*, Academic Press, Vol. 3, 166 (1968).
[14] V. V. DANIEL, *Dielectric Relaxation*, Academic Press, London and New York (1967).